Infrared interferometry to spatially and spectrally resolve jets in X-ray binaries

Markoff, S.; Russell, D.M.; Dexter, J.; Pfuhl, O.; Eisenhauer, F.; Abuter, R.; Miller-Jones, J.C.A.; Russell, T.D.

DOI
10.1093/mnras/staa1193

Publication date
2020

Document Version
Final published version

Published in
Monthly Notices of the Royal Astronomical Society

Monthly Notices
of the
ROYAL ASTRONOMICAL SOCIETY

MNRAS **495,** 525–535 (2020)
Advance Access publication 2020 April 30

doi:10.1093/mnras/staa1193

Infrared interferometry to spatially and spectrally resolve jets in X-ray binaries

Sera Markoff [1]★ David M. Russell [2] Jason Dexter [3,4] Oliver Pfuhl,[5] Frank Eisenhauer,[4] Roberto Abuter,[5] James C.A. Miller-Jones [6] and Thomas D. Russell [1]

[1]*Anton Pannekoek Institute for Astronomy and GRAPPA, University of Amsterdam, Science Park 904, 1098 XH Amsterdam, the Netherlands*
[2]*Center for Astro, Particle and Planetary Physics, New York University Abu Dhabi, P.O. Box 129188, Abu Dhabi, UAE*
[3]*JILA and Department of Astrophysical and Planetary Sciences, University of Colorado, Boulder, CO 80309, USA*
[4]*Max Planck Institute for Extraterrestrial Physics (MPE), Giessenbachstr. 1, D-85748 Garching, Germany*
[5]*European Southern Observatory, Karl-Schwarzschild-Str. 2, D-85748 Garching, Germany*
[6]*International Centre for Radio Astronomy Research – Curtin University, G.P.O. Box U1987, Perth, WA 6845, Australia*

Accepted 2020 April 23. Received 2020 April 23; in original form 2019 October 8

ABSTRACT

Infrared interferometry is a new frontier for precision ground-based observing, with new instrumentation achieving milliarcsecond (mas) spatial resolutions for faint sources, along with astrometry on the order of 10 microarcseconds (μas). This technique has already led to breakthroughs in the observations of the supermassive black hole at the Galactic centre and its orbiting stars, active galactic nucleus, and exo-planets, and can be employed for studying X-ray binaries (XRBs), microquasars in particular. Beyond constraining the orbital parameters of the system using the centroid wobble and spatially resolving jet discrete ejections on mas scales, we also propose a novel method to discern between the various components contributing to the infrared bands: accretion disc, jets, and companion star. We demonstrate that the GRAVITY instrument on the Very Large Telescope Interferometer should be able to detect a centroid shift in a number of sources, opening a new avenue of exploration for the myriad of transients expected to be discovered in the coming decade of radio all-sky surveys. We also present the first proof-of-concept GRAVITY observation of a low-mass XRB transient, MAXI J1820+070, to search for extended jets on mas scales. We place the tightest constraints yet via direct imaging on the size of the infrared emitting region of the compact jet in a hard state XRB.

Key words: accretion, accretion discs – instrumentation: interferometers – infrared: stars – X-rays: binaries.

1 INTRODUCTION

Radio wave interferometry has been in development for decades, culminating in the exquisite precision of Very Long Baseline Interferometry (VLBI). However as one goes to higher frequencies, atmospheric effects makes visibility corrections more challenging, requiring generally shorter integration times on any given source. In the optical/infrared (OIR) bands, the previous generation of instruments could only image very bright sources using interferometry (e.g. *V*- and *H*-band photometric magnitudes of $\leq$2; Monnier et al. 2007; Che et al. 2011). Current instrumentation includes the Navy Precision Optical Interferometer and the Center for High Angular Resolution Astronomy (CHARA) Array, which consist of 12 cm–2 m aperture telescopes with sensitivity limits on the order of 6–10 mag (ten Brummelaar et al. 2005; van Belle et al. 2019). The Keck Interferometer (e.g. Swain et al. 2003; Kishimoto et al. 2011) and Astronomical Multi-BEam combineR on the Very Large Telescope Interferometer (AMBER/VLTI) (Weigelt et al. 2012) observations with 8–10 m telescopes have pushed these limits to much fainter sources ($K \simeq 10$). Increasing the sensitivity to still lower fluxes and higher spectral resolution is desirable, since only interferometry provides the precision necessary to resolve individual components in the OIR for many astrophysical systems.

The newest frontier in OIR interferometry is fringe tracking and precision astrometry using a sufficiently bright star within a few arcseconds of the desired target. Without corrections, atmospheric effects cause too much jitter in the fringes to integrate for periods long enough to detect fainter sources. By phase referencing, the fringes of the target can be actively stabilized with respect to the reference source, allowing for integration times long enough that the target can be much fainter than the reference object. An instrument with these capabilities is now in operation on the VLTI, GRAVITY (Gravity Collaboration et al. 2017a).

GRAVITY is a second generation interferometric instrument, commissioned on the VLTI in 2016. It allows observing two objects (one bright fringe-tracking, phase reference object and one fainter science object). When GRAVITY is used with the Auxiliary Telescopes (ATs, 1.8 m diameter) and the New Adaptive Optics Module for Interferometry (NAOMI), the brighter phase reference object must

★ E-mail: s.b.markoff@uva.nl

have an infrared magnitude of $K \leq 8$, and the faint object has to be within 4 arcsec from the bright object but can be as faint as $K \leq 12$–13. When GRAVITY is used with the Unit Telescopes (UTs; 8 m diameter), the bright object can be $K \leq 11$, and potentially even as low as $K \sim 12$ under good conditions. The faint object has to be within 2 arcsec, with a current limiting magnitude around $K \leq 19$ (Gravity Collaboration et al. 2017a, 2018b). The astrometric accuracy is as good as 20 μas in the best cases (Gravity Collaboration et al. 2017a, 2019b), with spectral differential astrometry demonstrated with a precision of 2 μas for high-mass X-ray binaries (HMXBs, Waisberg et al. 2017) and active galactic nucleus (AGN, Gravity Collaboration et al. 2018a). While the small separation between fringe-tracking and phase reference objects is a limitation for finding viable Galactic targets, we here discuss the potential new science cases particularly when considering planned upgrades allowing a separation of ∼30–40 arcsec.

The VLT point spread function for imaging is ∼ milliarcsecond (mas), thus the superb stability of GRAVITY allows the determination of relative motions in objects to precisions ∼100 times better than the resolution of their structure. GRAVITY was designed primarily to study orbital motions of stars or flare emission in the strong gravitational field of the supermassive black hole (BH) Sgr A* (Gravity Collaboration et al. 2020), and has provided the most accurate distance to the Galactic centre (Gravity Collaboration et al. 2018b, c, 2019b), as well as the first detection of an exoplanet by OIR interferometry (Gravity Collaboration et al. 2019a). However GRAVITY also has the potential to revolutionize XRB studies, and in fact has already been used to study the size, structure, and spectra of two Galactic HMXBs, GX 301−2 and SS 433 (Waisberg et al. 2017; Gravity Collaboration et al. 2017b; Waisberg et al. 2019a). While low-mass XRBs (LMXBs) are generally too small (for their distance) to be spatially resolved on mas scales using the IR band, an IR astrometric accuracy of ∼10 μas could enable the first direct detection of individual contributions to the IR spectrum, as well as an independent method for obtaining system orbital parameters.

In this paper, we propose a feasibility study for how IR interferometry, using GRAVITY in particular, can be exploited to separate emission components in XRBs and thus constrain accretion/outflow physics. In Section 2, we describe the scientific questions that IR interferometry can help address for XRBs, particularly transient microquasars. In Section 3, we explore the feasibility using several typical sources as a guide, particularly for observing faint targets off-axis. In Section 4, we present the first proof-of-concept, mas-scale IR interferometric observation of a Galactic transient XRB, MAXI J1820+070, using GRAVITY. Finally, in Section 5, we summarize and make some predictions for the coming decade of all-sky transient detections.

2 SCIENCE MOTIVATION

2.1 Spatially resolving jets in XRBs

VLBI studies of jets in nearby AGN such as M87 have revealed a spine and sheath geometry, as predicted by theoretical models (Perlman et al. 2011; Walker et al. 2018), as well as the collimation profile of the jet (e.g. Asada & Nakamura 2012). Such images can be used to constrain the equations of force balance (i.e. internal versus external pressure), while variability provides information about turbulence within the flow. M87 is in fact so close and large that the Event Horizon Telescope (global 1 mm VLBI with the Atacama Millimeter/submillimeter Array, ALMA, in phased-array mode at its core) was able to directly image the shadow of the BH (e.g. Event Horizon Telescope Collaboration et al. 2019).

While Galactic BH XRBs are much closer than AGN, they are typically millions to billions of times smaller, so direct imaging is a challenge and resolving the BH shadow or inner accretion disc is well beyond the capabilities of current facilities. With the advent of GRAVITY on the VLTI, however, there is an intriguing possibility to directly resolve expanding mas-scale jets in a transient XRB outburst, and to spectrally decompose the accretion components from each other as well as from the companion star. The advantage of XRBs compared to AGN is that one can observe millions more dynamical time-scales, thus obtaining constraints on the inner disc physics over much longer relative time-scales. Direct imaging provides the best insights into jet morphology, energetics, and interactions. Because one of the pressing questions at the moment in modelling accretion flows centres on how and where particles are energized (see e.g. Romero et al. 2017; Ball, Sironi & Özel 2018), the promise of pinpointing the moment when XRB jets launch and then begin to accelerate high-energy particles makes them extremely valuable testbeds for constraining theory.

2.1.1 *Compact jets and discrete ejecta*

XRBs exist as both persistent (mostly high-mass companions; HMXB) and transient (with low-mass companions; LMXB) sources, the latter of which experience periodic outburst cycles. Within a single outburst we witness the launching and quenching of jets, in some sources repeatedly on a few-year time cycle (e.g. Corbel et al. 2013). Until now direct imaging has focused on radio-VLBI techniques because of the phenomenal spatial resolution, but only three compact, steady jets associated with the non-thermal-dominated 'hard state' have been resolved with radio-VLBI to date: GRS 1915+105 (Dhawan, Mirabel & Rodríguez 2000), Cyg X−1 (Stirling et al. 2001), and MAXI J1836−194 (Russell et al. 2015). However during state transitions to the thermal/disc-dominated 'soft state', the jets transform dramatically, and increasingly more radio-VLBI studies have been able to resolve, and track the evolution of, discrete ejecta on mas scales (e.g. Mirabel & Rodríguez 1994; Hjellming & Rupen 1995; Tingay et al. 1995; Fender et al. 1999; Mioduszewski et al. 2001; Miller-Jones et al. 2011, 2019; Brocksopp et al. 2013; Rushton et al. 2017).

The compact jets seen in the hard state also emit IR synchrotron emission, but it originates from too close to the BH to be directly resolved (e.g. Russell et al. 2006; Gandhi et al. 2011; Buxton et al. 2012). During state transitions, discrete jet ejecta emit optically thin synchrotron from radio to IR, such that the IR flux is generally expected to be fainter than the radio (though see GRS 1915+105, Fender et al. 1997; Eikenberry et al. 1998). Despite this faintness, with the advent of fringe-tracking and phase referencing capabilities with VLTI via the GRAVITY experiment, it may be possible to image XRB jet activity in the IR similar to what has been done with radio-VLBI.

2.1.2 *Previous claims of OIR extended jets*

There have in fact been claims of a marginal IR detection of a compact jet of 0.2 arcsec in the source GRS 1915+105 (Sams, Eckart & Sunyaev 1996), however this has never been confirmed by later

detections. But recently, IR emission lines from plasma in the jets of the exotic Galactic XRB SS 433 have been spatially resolved with GRAVITY (Gravity Collaboration et al. 2017b). On larger scales, extended jets of XTE J1550−564 resolved on arcsecond–arminute scales, detected at radio and X-ray frequencies, were almost – but not quite – detected by the VLT at optical wavelengths (Corbel et al. 2002).

2.1.3 Detectability with GRAVITY: spatial scales

Because GRAVITY is capable of imaging structures on spatial scales of ∼1–50 mas (corresponding to, e.g. ∼0.3–20 au for a source at 3 kpc; up to ∼60 au at 8 kpc), transient features such as ejecta or jet–ISM (interstellar medium) interaction regions may be now be detectable. Specifically, after transition to the soft state the core is no longer active but the ballistic ejecta are still moving. Based on the radio-VLBI observations, we expect these bright ejecta to be spatially resolved with GRAVITY, with motions of ∼10s–100 mas d^{-1} (note that extremely fast motions of 100 mas d^{-1} could result in motion/smearing within a GRAVITY observation itself, depending on integration times).

The mas-scale jets seen with radio-VLBI are typically discrete ejecta that are themselves unresolved down to <1 mas (see table 1 in Miller-Jones, Fender & Nakar 2006), so we do not expect them to be resolved out. One could therefore use a *uv* binary source model (XRB core and jet ejection, see Section 4.1 and Fig. 3) to identify spatially resolved ejecta on scales of 1–50 mas. In the case of a nearby source with high velocity ejecta, the mas-scale ejections could move on time-scales as short as the exposure time. For these, if the movement is comparable to or longer than the integration time (tens of minutes), these will be detectable. A good example of this is the detection of the resolved S2 star from Sgr A*, in which the dynamical time-scale was shorter than the integration time, yet the *uv* model fitting was successful (Gravity Collaboration et al. 2018c, 2019b, 2020).

2.1.4 Detectability with GRAVITY: fluxes

For a typical XRB, the radio flux densities of discrete ejecta on the 1–50 mas size scales we can probe with GRAVITY are on the order of 10–500 mJy (at 15 GHz, e.g. Fender, Homan & Belloni 2009; Miller-Jones et al. 2019). Assuming a standard optically thin spectrum ($\alpha = -0.6$ to -0.8) would predict a $K \sim 10$–12 mag core and a $K \sim 15$–16 mag discrete ejection, meaning GRAVITY could significantly detect and resolve both components. Because such discrete ejecta would likely be several magnitudes fainter than the compact jet, and the unresolved accretion disc and (in some cases) the star, mas-scale discrete ejecta at these fluxes would never have been noticed before in any IR data.

2.1.5 Detectability with GRAVITY: brief, brighter jets

There may also be bright IR discrete ejecta that are tens of mJy (K∼10 mag), but only briefly near the start of the hard-to-soft state transition, before fading to similar or fainter flux later in the radio. For example, the non-spatially resolved jet flares in GRS 1915+105 were a similar flux density (in Jy) in IR and radio, with radio occurring minutes later than IR (Fender et al. 1997; Mirabel et al. 1998). Both IR and radio flares lasted ∼20 min, strongly suggesting adiabatic losses dominating. However during V404 Cyg's latest outburst, Tetarenko et al. (2017) found that 7 Jy submm flares lasting tens of minutes to an hour at 666 GHz were followed by only ∼1 Jy flares in the radio bands. Such flares may have very brief, transient IR counterparts of a few hundred mJy ($K \lesssim 9$ mag) or more, lasting time-scales of minutes to tens of minutes. To date no such IR flare has been resolved in a typical BH transient (GRS 1915+105 is considered an outlier), but they may have been missed due to low sampling or short integration times. Such ejecta are likely to emit between $K \sim 9$–16 during the days/week just after launching. In one system, an IR flare peaking at $K < 13$ mag and lasting four days has been detected during state transitions, and may have been brighter on <1 d time-scales (Buxton & Bailyn 2004; Russell et al. 2020). Such flares, on hour–day time-scales – if present – will be detectable and spatially resolved if they have typical motions of ∼10s–100 mas d^{-1}. However, we note that for very rapid flares which change flux on time-scales comparable to a single observation, this could introduce image artefacts. As such, the flux variability would likely preclude all but the most basic binary model fitting in these cases.

2.1.6 Consequences of a detection

A clear detection would allow constraining the location, velocity, size/morphology, and evolution of the IR jets. Together with radio-VLBI observations, an IR detection will also provide information about the radiating particle energy distribution of the mas-scale discrete ejecta. Any early-time, bright IR detections would be crucial for constraining the launch time of the jets, for comparison to X-ray timing signatures associated with this launching (see e.g. Miller-Jones et al. 2012), as they are less affected by optical depth effects. Finally, when the steady jet re-establishes itself before the outburst ends, GRAVITY could be used to investigate changes in the inner jet and movement of any interaction hotspots.

2.2 Spectral decomposition using interferometry

While challenging, IR interferometry offers an exciting new dimension to the multiwavelength studies currently used to deconstruct the physics driving accretion and outflows.

Our understanding of XRB accretion physics has evolved significantly over the last decades, mainly due to the monitoring of entire outburst cycles in the X-ray bands via triggered instruments such as the *Rossi X-ray Timing Explorer*, *SWIFT*, and more recently, the *Neutron Star Interior Composition Explorer Mission (NICER)* (e.g. Belloni et al. 2005; Muñoz-Darias, Motta & Belloni 2011; Motta et al. 2017; Stevens et al. 2018). These observations have led to a greater understanding of the disc/jet coupling driving the discrete accretion states (e.g. McClintock & Remillard 2006; Belloni 2010) that are most pronounced in BH XRBs, the main focus of this work. The frontier has now shifted to the lower frequency bands, as simultaneous triggering of radio and OIR observations with the X-rays has revealed a parallel evolution in the interplay between the accretion inflow in the accretion disc, jet outflows, and sometimes the stellar companion.

The OIR bands in particular offer a valuable new testbed for many aspects of accretion physics in XRBs, as they can be comprised of multiple contributions from the accretion disc, jets, and star, the former of which can exchange dominance during state changes. For instance, in the soft state, the outer regions of the accretion flow can reradiate emission from the inner zones in the OIR bands, as can the companion star itself (e.g. O'Brien et al. 2002; Hynes 2005; Migliari et al. 2007). In the hard state it is now well established that synchrotron emission from the jets extends into the OIR bands (e.g. Corbel & Fender 2002; Russell et al. 2006, 2010; Buxton et al. 2012;

Saikia et al. 2019), either as an extension of the flat/inverted, self-absorbed spectrum, or beyond the synchrotron self-absorption break as an optically thin power law. The break itself has been explicitly resolved in some observations (e.g. Migliari et al. 2006; Gandhi et al. 2011; Russell et al. 2013) and recent simultaneous broad-band campaigns of XRBs in outburst demonstrate that the break dynamically moves up and down in frequency through the band (Russell et al. 2014, Russell et al. 2020).

Understanding the contribution of the jets in the IR and in particular, whether the IR is above or below the break, or how the break evolves, has become a key focus of XRB studies as this places strong constraints on the jet geometry, dynamics, and energetics. For instance, recent multiwavelength variability studies have revealed a characteristic size scale for this break (Gandhi et al. 2017; Paice et al. 2019), as well as very strong near-IR to mid-IR variability from the compact jets (Gandhi et al. 2011; Baglio et al. 2018; Vincentelli et al. 2018; Malzac et al. 2018). Similarly the first ever IR quasi-periodic oscillations (QPOs) with a harmonic of the X-ray QPO frequency (Kalamkar et al. 2016) reveal the tight coupling of jet to disc. If the spectral slope beyond the break can be constrained, this also helps determine the particle acceleration properties and together with limits from the X-rays and γ-rays, the maximum radiative power of the jets (see e.g. Laurent et al. 2011; Corbel et al. 2012; Zdziarski et al. 2014; Rodriguez et al. 2015; Zanin et al. 2016; Espinasse et al. 2020). However, the clear evidence for multiple contributions to the OIR (see e.g. Homan et al. 2005; Buxton et al. 2012; Baglio et al. 2018) can make identifying the OIR jet contribution challenging.

Isolating the jet contribution to the OIR spectrum is therefore a key new milestone for understanding XRB jet physics in general, and gauging their total power budgets (Corbel et al. 2002; Gallo et al. 2005; Abeysekara et al. 2018). Furthermore, because of the increasing body of evidence that the accretion physics in XRBs and AGN scales predictably with mass (Merloni, Heinz & di Matteo 2003; Falcke, Körding & Markoff 2004; McHardy et al. 2006; Plotkin et al. 2012; Koljonen et al. 2015; Connors et al. 2017), constraints found from IR studies of XRBs will cast light on larger scale issues in galactic evolution such as the physics governing jet launching and power, and eventually energy released into the environment.

3 FEASIBILITY STUDY FOR A NEW APPLICATION OF IR INTERFEROMETRY TO XRBS

As typical XRBs have binary separations falling in the range of 1–100 μas, they are not directly resolvable with the VLTI, but the system motion should be detectable. The simplest, but potentially one of the most important, applications of the VLTI for XRBs is the search for a wobble in the light centroid position, which can be used to constrain the mass function of the system. Many systems now have accurately measured orbital periods but the mass of the compact object and/or companion star are, on the whole, poorly constrained. Since the orbital separation, $a \propto P^{2/3}(M_1 + M_2)^{1/3}$ where P is the orbital period, we can therefore solve for the total system mass with precise determinations of a and P.

For objects with several good reference stars in the field, the VLTI can in principle be used to further constrain the system orientation (in projection on the sky) and inclination. The amount of orbital wobble measured, for non-zero inclination systems, will depend on the angle between the orbital plane of the XRB and the reference star. By measuring the wobble using a number of reference stars at different angles from the XRB, a solution for the orientation of the disc and apparent eccentricity on the plane of the sky can be derived. While for eccentric orbits, speeds will vary from periastron to apastron, the orbits of most XRBs (at least Roche lobe overflow LMXBs) are circular, and in all cases the inclination angle of the system can also be constrained. If the stellar companion type and mass is known, as is the case for sources with a measured mass function in quiescence, the physical parameters of the system can be completely characterized using this approach.

If both the orientation of the orbital plane as well as the inclination can be constrained, a further interesting test is to compare these with the observed orientation of the radio jets (which are generally well known for most of the prime candidate sources considered in this paper). Such a test could help identify more systems with drastically misaligned jets similar to the 'microblazar' V4641 Sgr (Hjellming et al. 2000; Orosz et al. 2001; Maccarone 2002). The existence of significant numbers of misaligned jets would help constrain the extent to which jet axes align more with the BH than the outer disc, as predicted by Rees (1978) and now reproduced numerically (e.g. Liska et al. 2018), and enable a study of time-scales for which the Bardeen–Petterson effect (Bardeen & Petterson 1975) could bring the jets back into alignment.

3.1 Centroid shift and potential target list

The most challenging but potentially most exciting detection beyond orbital effect would be a shift in the image centroid as a function of accretion state, driven by waxing and waning in the three main system components in the IR band. Understanding the orbital period via the wobble technique or otherwise will be a necessary first step, to allow comparison of the source at the same orbital phase in different states, and potentially to co-add images from several orbits. A schematic of how this technique would work to identify the jet contribution can be seen in Fig. 1. If the system is observed at the same orbital phase during the hard and soft states respectively, and the binary separation is sufficiently large, the shift in centroid position should be detectable for a few systems with GRAVITY. If significant IR emission is thought to be contributed from irradiation in the star, this technique together with spectral modelling would also help to break the degeneracy between that and disc/jet, if comparisons are made between state changes.

For both HMXB and LMXB, astrometry with the current specifications of GRAVITY on the VLTI should be achievable if the target has $K \lesssim 16$ and another $K \lesssim 11$ mag star lies within 2 arcsec from the target, or vice versa (brighter target, fainter reference star). For our specific interests, transient LMXBs (or bright flares in persistent LMXBs) are preferable, but in Table 1, we provide a list of all the best known sources which would be good candidates based on the best known estimates of distance, orbital period, and component masses from the literature to calculate the orbital separation. Starting from the 40 XRBs with radio detections (i.e. evidence of jets), we find 15 that have apparent orbital separations on the sky $a > 10\,\mu$as (in descending order of a). We include sources too far north for the VLT such as the HMXB Cyg X−1, because it is a canonical object with well-constrained physical parameters that could be useful for future interferometry instruments (on a northern interferometer such as the Large Binocular Telescope, the CHARA Michelson Array, and the Magdalena Ridge Observatory Interferometer; Angel et al. 1998; ten Brummelaar et al. 2005; Buscher et al. 2013; Gies et al. 2019).

These are mostly LMXBs (including BH and neutron star sources) and also some HMXBs with radio emission. We consider these the current best targets for VLTI attempts with GRAVITY (except for three sources that are too far north, shown in italics in the table); we do not include the other systems in the table as they have smaller

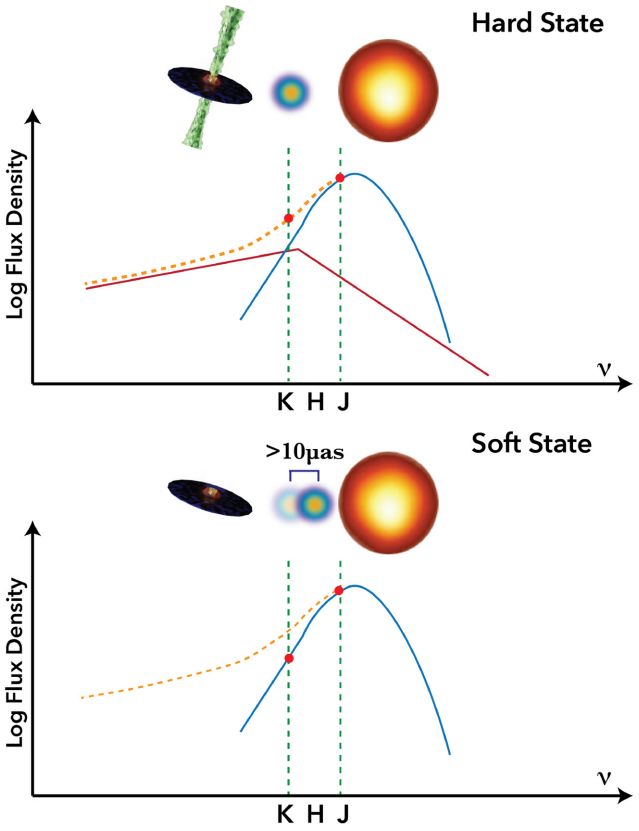

Figure 1. Schematic of the centroid shift expected during state changes, due to the disappearance of the jet IR synchrotron emission. Top: system in the hard state of a LMXB, where both jet (red broken power law) and companion star (blue blackbody) contribute comparably to the flux density in the IR bands (orange dashed). Bottom: same system, at the same orbital phase, after transitioning to the soft state and jet contribution to the IR is quenched, resulting in a shift of the image centroid towards the companion star in the *K* band. The orbital wobble, most prominent when the star is producing the IR emission, is largely reduced when the jet is dominating. Note that another centroid shift could be potentially seen between *K* and *J* bands during state transitions.

apparent orbital separations on the plane of the sky, and are more challenging for GRAVITY. The observed (not de-reddened) *K*-band magnitudes are also tabulated, as are the number of $K < 12$ stars within 40 arcsec of the XRB, listed in the Two Micron All Sky Survey (2MASS) catalogue. The reason this list extends beyond GRAVITY's current beam-forming capabilities is because of the proposed enhanced sensitivity and the enlarged field of view of a possible GRAVITY+upgrade (in preparation), that was presented at the 'The Very Large Telescope in 2030' conference, ESO Garching, 2019 June 17–20. All of these objects also have radio flux densities (not shown) which can be used to extrapolate a first-order estimate of the expected IR flux from the jets. In some cases the jet contribution to the *K*-band IR emission has been estimated in the hard state; for these we estimate the phase shift of the centroid between jet on and off (if instead the star dominates) states. If instead the shift is from jet to accretion disc over the transition, there would be no phase shift in the XRB during such a transition (this is most likely the case for the LMXBs with the faintest companions, such as GX 339−4, XTE J1550−564, and Cen X−4) and so the phase shift calculated from the ratio $\frac{I_j}{I_j+I_s}$ (see below) represents an upper limit in these systems. However in many of the sources in Table 1, the star is large and brighter than (or of comparable brightness to) the accretion flow (GX 301−2, CI CAM, Cyg X−1, SS 433, GRS 1915+105, V4641 Sgr, and GRO J1655−40 as shown in Fig. 1, e.g. Kaper et al. 1995; Miroshnichenko et al. 2002; Migliari et al. 2007; Hillwig & Gies 2008; van Oers et al. 2010; Rahoui et al. 2011; MacDonald et al. 2014; Russell & Shahbaz 2014) and so a phase shift is expected.

There are currently at least six known systems with orbital separations $a > 50\,\mu$as, which would yield a 5σ detection with GRAVITY of an astrometric shift over the orbital period. This shift also depends on the mass ratio; for systems in which the BH mass is much greater than the companion mass, the orbital wobble of the companion could be as large as twice the orbital separation. Most orbital periods of the sources in Table 1 are days to weeks. Exoplanets, by comparison have periods on the order of years, so instrument drifts and systematics over the longer time frame introduce additional astrometric errors which are not relevant for microquasars.

Unfortunately, none of the targets in Table 1 have known nearby stars within 2 arcsec in 2MASS, with the closest being GRS 1915+105 with a $K = 13.2$ star 3.3 arcsec from the target. However, a faint star close to the brighter XRB would not be easily detectable in the 2MASS survey, so it is possible some close stars have been missed by 2MASS. We did also check higher resolution images from Visible and Infrared Survey Telescope for Astronomy (VISTA) surveys (Minniti et al. 2010, including VVV and VHS) for nearby stars. If off-axis capabilities allow a phase reference star within ∼30–40 arcsec (as suggested in a GRAVITY+ white paper; Gravity Collaboration et al., in preparation), this dramatically increases the feasibility. Most targets have several (up to 17) bright $K < 12$ 2MASS stars within 40 arcsec (Table 1). GX 301−2 and CI Cam have the widest angular orbital separations, but in both these systems the jets never brighten to an IR flux level comparable to that of the companion star. Some of the other sources do have relatively bright jets though, and we investigate these further below.

The spacing of an interferometer's fringes on the sky is λ/B (where B is the baseline length), analogous to the λ/D resolution of a single optical telescope. The phase of the centroid of the compact object (dominated by either the jet or the disc, we will use the jet as an example below) and companion star can be calculated from:

$$\phi = 360^\circ \frac{I_j}{I_j + I_s} \left(\frac{2\pi a_\mathrm{r}}{\lambda/B} \right), \quad (1)$$

where a_r is the binary separation in radians and I_j and I_s are the measured jet and star flux at a given frequency, respectively. This equation assumes (i) $2\pi a_\mathrm{r} \ll \lambda/B$ (the marginally resolved limit), (ii) the angle between the line connecting the XRB and guide star on the sky and the projection on the sky of the line connecting the two telescopes, is zero (this geometry gives the highest resolution; cos(angle) = 1), and (iii) sin $a_\mathrm{r} \approx a_\mathrm{r}$, which is valid for the small angles we are dealing with here. The ratio λ/B for *K*-band is 4.37 mas (we adopt a baseline of 110 m for the VLTI). For an XRB with an orbital separation on the sky of $a_\mathrm{r} = 100\,\mu$as, the maximum phase shift between the hard and soft states (due to jet quenching) is on the order of $\delta\phi \sim 8^\circ$, which corresponds to ∼100 μas on the sky (i.e. the orbital separation), and thus should be detectable with GRAVITY. This maximum shift scenario, in which the jet or disc produces ∼100 per cent of the flux in the hard state and the star produces ∼100 per cent of the flux in the soft state, will generally not be the case in reality. We therefore estimate the phase shift using the ratio $\frac{I_j}{I_j+I_s}$ and these are given in Table 1. The estimates of this ratio are taken from the literature using the relative jet and star contributions at the frequency of *K* band (Fender et al. 1997; Migliari et al. 2007;

Table 1. The XRBs (with radio detections) possessing the widest orbital separations on the sky[1] (all with $a > 10\,\mu$as). The best interferometry candidates are those that are expected to have a shift of the phase of the centroid due to a changing IR jet contribution (final two columns).

Source[2]	BH/NS[3]	K (mag)	a (μas)[4]	$K < 12$ stars[5] within 40 arcsec	References	$\frac{I_j}{I_j+I_s}$	$\delta\phi$
GX 301−2 (BP Cru)	NS	5.7	243 ± 15	3 stars, $K = 6.7$–10.5	1–2	–	–
CI Cam	?	4.1–4.7	223 ± 176	1 star, $K = 10.2$	3	–	–
Cyg X−1	BH	6.5	127 ± 16	1 star, $K = 8.9$	4	0.006	(0.07 ± 0.01)°
SS 433	BH?	8.2	75 ± 7	0 stars	5–6	–	–
V404 Cyg	BH	7.7–12.5	61 ± 5	4 stars, $K = 9.5$–11.8	7	>0.80	(4.8 ± 0.9)°
GRS 1915+105	BH	11.4–13.5	55 ± 14	6 stars, $K = 9.0$–12.0	8	0.05–0.2	(0.68 ± 0.51)°
Flaring state						∼1	(4.7 ± 1.2)°
GX 13+1	NS	11.9–12.6	44 ± 8	17 stars, $K = 6.9$–12.0	9–10	–	–
Cir X−1	NS	7.2–11.9	28 ± 11	10 stars, $K = 9.8$–11.9	11–14	–	–
GRO J1655−40	BH	11.0–13.3	25 ± 3	10 stars, $K = 9.1$–12.0	15–16	0.25	(0.53 ± 0.05)°
A0620−00	BH	9.9–14.5	17 ± 2	0 stars	17–18	–	–
Cen X−4	NS	<13.0–14.8	16 ± 5	1 star, $K = 10.8$	19–21	–	–
V4641 Sgr	BH	12.7–13.7	13 ± 2	4 stars, $K = 8.3$–10.9	22–23	≳0.9	(1.1 ± 0.2)°
XTE J1550−564	BH	13.0–17.4	13 ± 2	7 stars, $K = 9.3$–12.0	24	0.9	(1.0 ± 0.2)°
GRO J1719−24	BH	<13.5–18.3	>12 ± 5	4 stars, $K = 8.0$–11.9	25–26	–	–
MAXI J1820+070	BH	9.5–15.1	>9 ± 1	1 star, $K = 12.0$	27,28	>0.5	>0.4°

Notes: [1]We do not include γ-ray binaries in this table, which are not thought to have extended jets. [2]Sources in **bold** have been observed with GRAVITY on VLTI; sources in *italics* are too far north for the VLTI (Dec. >+25°). [3]BH = black hole and NS = neutron star. [4]Errors on the estimated values of orbital separation are propagated from the errors in d, P, M_1, and M_2 (if the mass of the neutron star is not known we adopt $M_2 = 1.4 \pm 0.6\,M_\odot$). For GRO J1655−40, the value of a is given for distance 3.2 ± 0.3 kpc (Gandhi et al. 2019). [5]The number of $K < 12$ stars within 40 arcsec of the XRB, and their range of magnitudes (data from the 2MASS catalogue). The K-band jet contributions in the hard state are estimated from (in some cases modelling of) spectral energy distributions in Fender et al. (1997, 2000, 2018), Russell et al. (2006, 2010, 2013, 2018), van Oers et al. (2010), and Migliari et al. (2007). The references for the distances, orbital periods, and masses can be found in the following articles and references therein: (1) Tomsick & Muterspaugh (2010); (2) Doroshenko et al. (2010); (3) Thureau et al. (2009); (4) Orosz et al. (2011b); (5) Blundell, Schmidtobreick & Trushkin (2011); (6) Lopez et al. (2006); (7) Khargharia, Froning & Robinson (2010); (8) van Oers et al. (2010); (9) Corbet (2003); (10) Corbet et al. (2010); (11) Clarkson, Charles & Onyett (2004); (12) Jonker & Nelemans (2004); (13) Török et al. (2010); (14) Jonker, Nelemans & Bassa (2007); (15) Greene, Bailyn & Orosz (2001); (16) Gandhi et al. (2019); (17) González Hernández & Casares (2010); (18) Cantrell et al. (2010); (19) Shahbaz, Watson & Dhillon (2014); (20) Chevalier et al. (1989); (21) Hammerstein et al. (2018); (22) Orosz et al. (2001); (23) MacDonald et al. (2014); (24) Orosz et al. (2011a); (25) Masetti et al. (1996); (26) della Valle, Mirabel & Rodriguez (1994); (27) Torres et al. (2019); and (28) Atri et al. (2020).

van Oers et al. 2010; Russell et al. 2010; Chaty, Dubus & Raichoor 2011; Russell et al. 2013, 2018; Russell & Shahbaz 2014; Bernardini et al. 2016; Maitra et al. 2017).

To test the feasibility of this new class of measurement, we use some examples of known Galactic XRBs where the binary separation and broad-band spectral energy distribution are well constrained, allowing an estimation of the potential centroid shift. In Fig. 2, we show an example simultaneous, broad-band spectrum from the Galactic transient GRO J1655−40, which we have chosen because of its large orbital separation, the fact that in the hard state the jet flux is a reasonable fraction of the K-band flux, and that jet models have been fitted to this data set (Migliari et al. 2007, note that the conclusions would not be affected if the jet synchrotron cuts off well before the X-ray band). This source is visible to the VLT though it has currently returned to quiescence, but during outburst had a K-band magnitude of 11. We have calculated the predicted shift assuming the jet is entirely quenched in the K band during the soft state (this is supported by the dramatic quenching of radio and mid-IR flux in the soft state of GRO J1655−40; Migliari et al. 2007). Based on the spectrum, the jet contributes ∼25 per cent of the total flux in the hard state, leading to a predicted shift in phase of $\delta\phi = 0.5°$, which is in the detectable range by GRAVITY during a future outburst. There are 10 field stars brighter than $K = 12$ within 40 arcsec of GRO J1655−40, but none within 2 arcsec. If the field of view for phase referencing could be increased to >30 arcsec, a full orbital solution would be possible for this source.

The 'persistent transient' GRS 1915+105 is another interesting potential target, having been in an outburst state associated period-

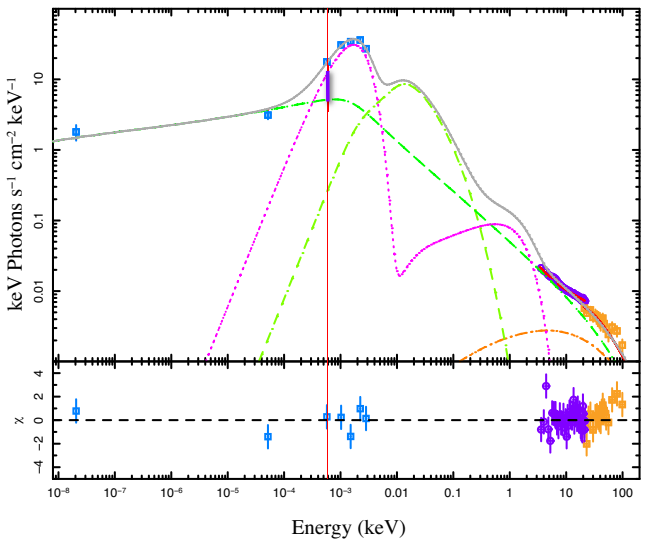

Figure 2. An example simultaneous, broad-band spectrum from GRO J1655−40 in the hard state, from Migliari et al. (2007), illustrating the K band (vertical red line) and the difference in flux between the jet synchrotron emission (dashed green line) and thermal companion star (dashed purple line; note the accretion disc is also present but very distinct at higher energy).

ically with jet ejections for the last 20+yr. During these flares, the jet produces almost all of the *K*-band flux, and the estimated shift in phase of the centroid is $\delta\phi \sim 5^\circ$.

We should also consider spectro-astrometry. GRAVITY provides a spectral range between 2.00–2.45 μm. The astrometric shift between blue *K* band (larger star contribution, in the case of GRO J1655−40) and red *K* band (dominated more by the jet) is larger than the astrometric shift of the average *K* band from photometry. It may be possible to distinguish features in the spectrum from regions dominated by the jet, disc and companion star. For example, a strong Br-γ line is expected from the accretion disc, various absorption lines from the companion star, and the red part of the *K*-band continuum dominated by the jet. If so, this would also give an interesting astrometric signal of different components at different positions. This has been recently achieved for SS 433, in which emission lines from the jets were found to be spatially offset from the continuum, the jets resolved at ∼1–10 mas scales (Gravity Collaboration et al. 2017b; Waisberg et al. 2019b), but this is the only known source with optical and IR emission lines from the jets.

In the last two columns of Table 1, we show the fractional jet contribution, and calculate the centroid phase shift, based on spectra taken from the literature for several of the best candidates. The errors on the phase are propagated from the errors in a and (for three sources) the jet contribution (if it is poorly constrained). Cyg X−1 has the widest orbital separation on the sky for sources with a jet contribution (making it a prime target for measuring the orbital wobble), but since it is an HMXB its IR flux is dominated by the companion, and the jet contributes just ∼0.6 per cent of the *K*-band flux at most. The predicted shift in the phase of the centroid due to the jet quenching is therefore small for Cyg X−1. In contrast, the IR jet flux of V404 Cyg was at least ∼80 per cent in the hard state during its outburst in 1989 (and possibly during the flares during the 2015 outburst; see e.g. Maitra et al. 2017), and the resulting phase shift is large; ∼5°. Both Cyg X−1 and V404 Cyg are located too far north to be observable from the VLTI, however it is likely that XRBs with similar orbital parameters and jet contributions (to the latter transient source at least) will be discovered in the coming years. A recent example is MAXI J1820+070, which was discovered in 2018 and has an orbital separation of $a > 10\,\mu$as (Table 1). We discuss the first GRAVITY observation of this source in the next section. A good target, observable from VLTI, is GRS 1915+105. During its flaring state the jet produces almost all of the IR emission, so we predict a centroid phase shift of $\delta\phi \sim 5^\circ$. The three remaining sources with measured IR jet contributions have predicted phase shifts due to a changing jet contribution of ∼0.3°–1°, making them the next best currently known sources visible from the VLTI.

3.2 Accounting for parallax and proper motion

This technique requires measuring changes in the centroid at the 10 μas level, on time-scales of hours–days (for abrupt state changes) to weeks–months (orbital modulation, co-adding images from several orbits). Parallax and proper motion will therefore be significant, and their effects will need to be removed, before centroid shifts from orbital motion and state changes can be detected with sufficient accuracy (see e.g. Tomsick & Muterspaugh 2010; Atri et al. 2019, for discussions on this related to XRBs). The targets in Table 1 with estimated centroid phase shifts due to a changing IR jet contribution have known parallax and proper motions measured from *Gaia* and/or radio VLBI (Gandhi et al. 2019; Atri et al. 2020, and references therein). The uncertainties on these measurements are ± 0.02–0.11 mas for the parallax and ± 0.05–0.22 mas yr^{-1} for the proper motion (all except XTE J1550−564 have measurements). By the time of the GRAVITY upgrade, these uncertainties will very likely be smaller, with updated values from subsequent *Gaia* data releases, and new VLBI observations.

Using these existing astrometric solutions, the positional uncertainties for any given epoch are of order 0.11–0.60 μas due to uncertainties in the parallax and 0.14–0.60 μas d^{-1} due to uncertainties in the proper motion (for parallax this will vary depending on location of the target on the sky and the time of year). Star-spots on the surface of the companion could also produce light centroid jitter, with a maximum centroid shift of the order of a few μ-au, with only extreme cases from superflares of some stars producing shifts up to ∼100 μ-au (e.g. Morris et al. 2018), or 0.02 $R_\odot$, or 0.1 μas at a distance of 1 kpc. This effect of star spots is much smaller than the other uncertainties discussed here. The hotspot/stream impact point can make a small contribution to the optical emission in quiescence (Cherepashchuk et al. 2019). The hotspot is only significant in some LMXBs (not HMXBs) in quiescence as an additional thermal emitter to the optical continuum, and emission lines, but in outburst these are negligible. Since we are interested in the *K*-band continuum, and the disc dominates the thermal emission in outburst, the hotspot will play an insignificant role in the *K*-band continuum. Considering these arguments, an abrupt jet contribution change on day time-scales at the $>10\,\mu$as level will be easily detectable over the smoother changes in target position due to parallax and proper motion. Over a period of a month, the uncertainties grow to 3–18 and 4–18 μas, which becomes significant for measuring orbital and state changes on the 10 μas level. However, with sufficiently accurate measurements from *Gaia* and VLBI, it will be possible to remove these effects. In addition, if enough GRAVITY measurements are made over year time-scales, it may be possible, to independently measure parallax and proper motion using GRAVITY. This would be extremely interesting for constraining the distances, Galactic distribution, natal kicks, and origins of the systems (e.g. Mirabel et al. 2001; Miller-Jones 2014; Atri et al. 2019).

Centroid shifts on the 10 μas level also require these target phase shifts to be measured relative to a phase calibrator source. The reference source is typically a star, which has its own parallax and proper motion. One will therefore need to determine the relative parallax and proper motion signatures between the reference star and the target. For the comparison star 2MASS J19053212−0016155 used below with the observation of MAXI J1820+070, we see that it has parallax and proper motion measured by *Gaia* DR2, with uncertainties of 0.051 and 0.076 mas yr^{-1}, respectively. These are very similar to our targets above, and will also be improved with future *Gaia* releases. One may choose to select reference stars with smaller uncertainties; perhaps more distant stars. For sufficiently high precision astrometry to measure orbital shifts, the systematic uncertainties related to the calibrator throw from the reference star should also be known. While these are believed to be negligible for the current few-arcsecond calibrator throw, they may become important for a wider field GRAVITY upgrade. We note that for many past and current GRAVITY science cases, true off-axis astrometry to a reference source has not been required, since all extragalactic targets are typically much further than our targets and therefore have negligible proper motion and parallax.

4 FIRST GRAVITY DETECTION OF A GALACTIC TRANSIENT XRB

As an initial proof-of-concept we here present the first triggered observation of a transient XRB with GRAVITY. MAXI J1820+070 is a new BH candidate XRB that was first detected in 2018 March

by the MAXI all sky X-ray monitor and ASAS-SN optical transient survey (Tucker et al. 2018; Kawamuro et al. 2018; Denisenko 2018). During its outburst rise it became one of the brightest XRB transients to date, becoming the second brightest X-ray source on the sky after Sco X−1, likely owing to its proximity (2.96 ± 0.33 kpc, recently measured from radio parallax; Atri et al. 2020). Unlike most outbursts, which usually transition from the steady jet-dominated state (hard X-ray state) to the ballistic jet state (transition through the intermediate states), MAXI J1820+070 rose very quickly to its maximum brightness and stayed there for several months, remaining in the steady jet state, meaning that we had an excellent chance to observe a very bright nearby system, with K-band magnitude of $\geq$9.5 (Mandal et al. 2018). A flux density of 300 mJy was measured in the mid-IR from the VLT Imager and Spectrometer for mid Infrared (VISIR) on VLT UT3 (Russell et al. 2018).

We observed MAXI J1820+070 with GRAVITY on the VLT Interferometer, using all four UTs (DDT 2101.D-0517) on the night of 2018 May 31–June 1. The XRB was observed at 04:28–05:45 UT and 06:11–06:59 UT on June 1. A comparison star 2MASS J19053212−0016155 (HD 177631) was observed at 05:47–06:10 and 07:01–07:31. All observations were performed under photometric conditions, with a variable seeing of 0.6–0.9 arcsec. We first closed the loop of the Multi-Application Curvature Adaptive Optics (MACAO) visible adaptive optics systems on target with each telescope. We observed in low spectral resolution, placing the science fibre away from the target in order to increase flux in the fringe tracking fibre.

We acquired one (55 min on source, with 40 min of science exposure) GRAVITY observation of MAXI J1820+070, when a steady, compact jet was being launched. This observation was a success in terms of feasibility, working remarkably well on a technical level. Despite the source being faint, fringe tracking (Lacour et al. 2019) was possible for $\gtrsim$ 50 per cent of the total observation time, providing good data quality (for the comparison star, fringes found in all baselines). The data were reduced with the standard GRAVITY pipeline using the default settings (Lapeyrere et al. 2014).

4.1 Results

The GRAVITY data show calibrated squared visibilities (V^2, squared correlated flux normalized to the value at zero baseline) consistent with a constant value of $\simeq$0.8–0.85. There is no apparent drop with increasing spatial frequency, that is the source is unresolved. We obtain an upper limit to the source size by fitting a Gaussian source model separately to each exposure. We allow for a variable zero-baseline visibility level to allow for coherence loss. The measured sizes are very small, with an upper limit of Gaussian FWHM $\lesssim$ 0.1 mas. We measure closure phases on all triangles (Fig. 3, upper panel) which are consistent with 0 with an rms of $\simeq$1°. Closure phases of zero are expected for an unresolved source (Lachaume 2003).

A secondary component would show up as an oscillatory signal in the closure phases and from a limit $\lesssim$2° the flux ratio is $\lesssim$2 per cent for separations $\gtrsim$1 mas. This argues for an unresolved or marginally resolved source, no asymmetry, and possibly some additional (over resolved/extended) background flux, which reduces the visibility at short baselines.

The photometric flux is a factor ∼5.9 lower than the calibrator (K = 10.0), which implies the source magnitude was $K \sim 11.9$ at the time of observation. The most likely model for the source is an unresolved point source, and some extended background. In the acquisition camera, the H-band flux of the calibrator is a factor of ∼3.6 larger, which would correspond to $H \sim 11.4$. The unresolved

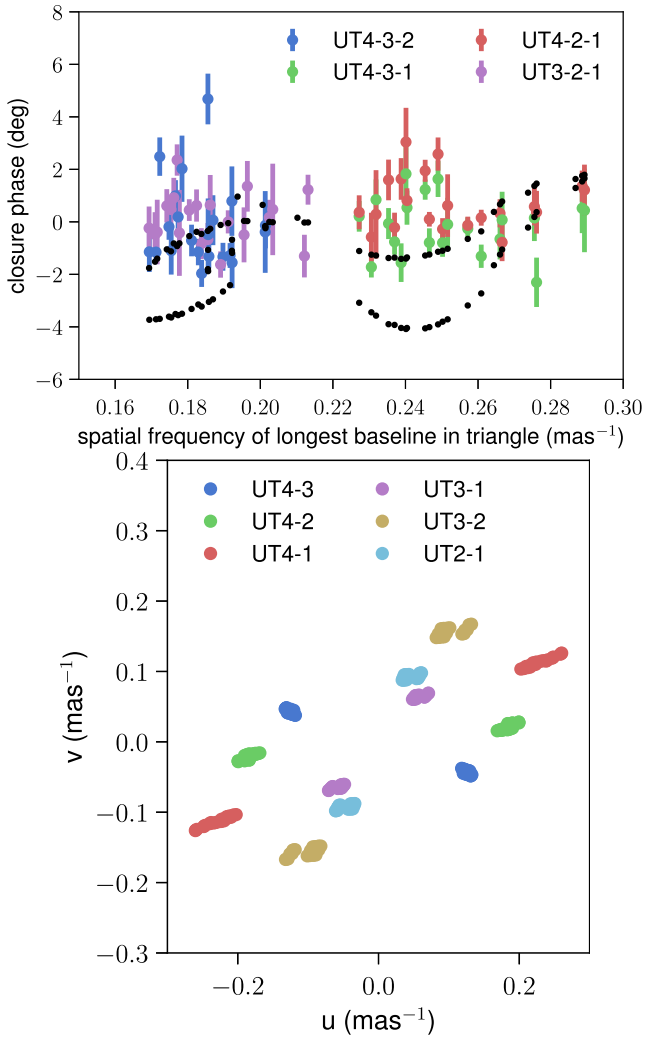

Figure 3. Measured closure phases (top) and *uv*-coverage (bottom) from our GRAVITY observation of MAXI J1820+070, coloured by baseline triangle or individual baseline. In the upper panel, coloured points with error bars are compared with the prediction of a binary model with a flux ratio of 0.03 and a separation of 10 mas at PA of 45° E of N (black dots). The measured closure phases constrain the flux ratio for any secondary ejected component to be 0.01–0.1 for separations 1–50 mas over all position angles. A single unresolved component would have closure phase = 0° at all spatial frequencies; our measured closure phases have median and rms 0.1 ± 1.5°, consistent with zero. The data are of sufficient quality to detect a faint, offset second component if present for a future transient.

core is fully consistent with expectations from jet models, as the IR synchrotron emission is likely dominated by regions within 10^3–10^4 r_g, where $r_g = \frac{GM}{c^2}$ is the gravitational radius of the BH (Gandhi et al. 2011, 2017). Nevertheless, there are no bright jet–ISM interaction sites, constraining the dissipation of energy associated with the steady jet on these scales. This observation was made during the prolonged hard state during the first part of the outburst of MAXI J1820+070. Later in the outburst, the source made a transition to the soft state, but unfortunately GRAVITY was unavailable at the time, and no observations of discrete ejecta were possible during this outburst.

Our size constraint is the the tightest direct (i.e. from imaging) limit on the size of the NIR emitting region in a hard state XRB. The source size limit of $\lesssim$0.1 mas corresponds to a distance of 4.4 × 10^7 km, or ∼5 × 10^6 r_g for a 5 $M_\odot$ BH at 3.0 kpc (Torres et al. 2019;

Atri et al. 2020, 5 $M_\odot$ is a lower limit; this source size estimate reduces for higher BH masses). While this size determination is less constraining than indirect methods, it agrees with those inferred from the variability time-scales (e.g. Casella et al. 2010; Kalamkar et al. 2016; Gandhi et al. 2017) and model predictions of XRB jet spectra (e.g. Markoff, Falcke & Fender 2001; Markoff, Nowak & Wilms 2005). The 0.5 mas size scale of the extended jet at radio wavelengths (Miller-Jones et al., in preparation) is comparable to the resolution of the GRAVITY observation at IR wavelengths, however the size scale of the steady, compact jet is expected to be orders of magnitude smaller at IR wavelengths. Nevertheless, this jet will be expanding and pushing into the surrounding ISM, and the fact that it was in the bright and steady jet state for two months means that the interaction zone with the ISM likely moved out to large scales. Conservatively estimating a velocity of the jet-head to be $0.01c$, this would be $\sim 10^{15}$ cm or $\sim 10^{-3}$ pc. At a distance of 3.0 kpc, this length-scale corresponds to tens of mas, well within the capability of GRAVITY. Our measurement is thus an excellent feasibility study and clearly demonstrates that spatially resolving jet ejecta and jet–ISM interaction regions on scales of 1–50 mas ($\sim$0.3–20 au for a source at 3 kpc; up to $\sim$60 au at 8 kpc) is possible with GRAVITY.

5 DISCUSSION

The case studies presented here demonstrate the untapped potential of upcoming high-precision OIR interferometry instruments such as GRAVITY to open a new discovery space for sources other than their intended targets. It is extremely timely to begin tests of this technique during commissioning of upgrades to GRAVITY for example, because current high-energy wide-field monitors (e.g. *Swift*, *Fermi*, and *MAXI*) are being joined by deeper X-ray all-sky instruments such as eRosita (Merloni et al. 2012), and the first generation of mid-to-high frequency range radio all-sky monitors (e.g. MeerKAT; Fender et al. 2017). We expect tens of new XRBs to be discovered in outburst, most of which will likely be in the Southern hemisphere and hence visible from the VLT. Well constrained orbital parameters for as many of these systems as possible will be vital for constraining the nature of the various compact primaries, as well as binary evolution models in general.

In the future, other more challenging applications can be considered. For instance, wavelength-dependent centroid shifts may be detectable when the contributions of two components in a single state are oppositely decreasing/increasing very quickly in the IR band. For instance, in the hard-to-soft state transition, the jet is likely dropping and the relative contribution of the thermal star or disc could be rising. By using, e.g. the Multi AperTure mid-Infrared SpectroScopic Experiment (MATISSE; Lopez et al. 2014) in combination with GRAVITY, a centroid shift between images in, e.g. the K and J bands could be detectable. We explored this idea briefly in an earlier conference presentation (Markoff 2008), and found that for most sources this shift would be a challenge to detect, however it is worth considering for the future generation of interferometers. The results would provide powerful constraints of particle acceleration efficiency and cooling in microquasar jets.

ACKNOWLEDGEMENTS

Based on observations collected at the European Southern Observatory under ESO programme ID DDT 2101.D-0517. SM is thankful for support from an NWO (Netherlands Organisation for Scientific Research) VICI award, grant number 639.043.513. JD was supported by a Sofja Kovalevskaja award from the Alexander von Humboldt Foundation and in part by NSF grant AST 1909711. JCAM-J is the recipient of an Australian Research Council Future Fellowship (FT140101082), funded by the Australian government.

REFERENCES

Abeysekara A. U. et al., 2018, Nature, 562, 82
Angel J. R. P., Hill J. M., Strittmatter P. A., Salinari P., Weigelt G., 1998, in Reasenberg R. D., ed., Proc. SPIE Conf. Ser. Vol. 3350, p. 881
Asada K., Nakamura M., 2012, ApJ, 745, L28
Atri P. et al., 2019, MNRAS, 489, 3116
Atri P. et al., 2020, MNRAS, 493, L81
Baglio M. C. et al., 2018, ApJ, 867, 114
Ball D., Sironi L., Özel F., 2018, ApJ, 862, 80
Bardeen J. M., Petterson J. A., 1975, ApJ, 195, L65
Belloni T., Homan J., Casella P., van der Klis M., Nespoli E., Lewin W. H. G., Miller J. M., Méndez M., 2005, A&A, 440, 207
Belloni T. M., 2010, in Belloni T., ed., Lecture Notes in Physics. Springer-Verlag, Berlin, 794, p. 53,
Bernardini F., Russell D. M., Kolojonen K. I. I., Stella L., Hynes R. I., Corbel S., 2016, ApJ, 826, 149
Blundell K. M., Schmidtobreick L., Trushkin S., 2011, MNRAS, 417, 2401
Brocksopp C., Corbel S., Tzioumis A., Broderick J. W., Rodriguez J., Yang J., Fender R. P., Paragi Z., 2013, MNRAS, 432, 931
Buscher D. F., Creech-Eakman M., Farris A., Haniff C. A., Young J. S., 2013, J. Astron. Instrum., 2, 1340001
Buxton M. M., Bailyn C. D., 2004, ApJ, 615, 880
Buxton M. M., Bailyn C. D., Capelo H. L., Chatterjee R., Dinçer T., Kalemci E., Tomsick J. A., 2012, AJ, 143, 130
Cantrell A. G. et al., 2010, ApJ, 710, 1127
Casella P. et al., 2010, MNRAS, 404, L21
Chaty S., Dubus G., Raichoor A., 2011, A&A, 529, A3
Cherepashchuk A. M., Katysheva N. A., Khruzina T. S., Shugarov S. Y., Tatarnikov A. M., Burlak M. A., Shatsky N. I., 2019, MNRAS, 483, 1067
Chevalier C., Ilovaisky S. A., van Paradijs J., Pedersen H., van der Klis M., 1989, A&A, 210, 114
Che X. et al., 2011, ApJ, 732, 68
Clarkson W. I., Charles P. A., Onyett N., 2004, MNRAS, 348, 458
Connors R. M. T. et al., 2017, MNRAS, 466, 4121
Corbel S., Coriat M., Brocksopp C., Tzioumis A. K., Fender R. P., Tomsick J. A., Buxton M. M., Bailyn C. D., 2013, MNRAS, 428, 2500
Corbel S., Fender R., 2002, ApJ, 573, L35
Corbel S., Fender R. P., Tzioumis A. K., Tomsick J. A., Orosz J. A., Miller J. M., Wijnands R., Kaaret P., 2002, Science, 298, 196
Corbel S. et al., 2012, MNRAS, 421, 2947
Corbet R. H. D., 2003, ApJ, 595, 1086
Corbet R. H. D., Pearlman A. B., Buxton M., Levine A. M., 2010, ApJ, 719, 979
della Valle M., Mirabel I. F., Rodriguez L. F., 1994, A&A, 290, 803
Denisenko D., 2018, Astron. Telegram, 11400, 1
Dhawan V., Mirabel I. F., Rodríguez L. F., 2000, ApJ, 543, 373
Doroshenko V., Santangelo A., Suleimanov V., Kreykenbohm I., Staubert R., Ferrigno C., Klochkov D., 2010, A&A, 515, A10
Eikenberry S. S., Matthews K., Morgan E. H., Remillard R. A., Nelson R. W., 1998, ApJ, 494, L61
Espinasse M. et al., 2020, ApJL, preprint (arXiv:2004.06416)
Event Horizon Telescope Collaboration et al., 2019, ApJ, 875, L1
Falcke H., Körding E., Markoff S., 2004, A&A, 414, 895
Fender R. et al., 2017, Proc. of "MeerKAT Science: On the Pathway to the SKA" (MEERKAT2016), Available at: https://pos.sissa.it/cgi-bin/reader/conf.cgi?confid=277, preprint (arXiv:1711.04132)
Fender R. P., Garrington S. T., McKay D. J., Muxlow T. W. B., Pooley G. G., Spencer R. E., Stirling A. M., Waltman E. B., 1999, MNRAS, 304, 865
Fender R. P., Homan J., Belloni T. M., 2009, MNRAS, 396, 1370
Fender R. P., Pooley G. G., Brocksopp C., Newell S. J., 1997, MNRAS, 290, L65

Fender R. P., Pooley G. G., Durouchoux P., Tilanus R. P. J., Brocksopp C., 2000, MNRAS, 312, 853
Gallo E., Fender R., Kaiser C., Russell D., Morganti R., Oosterloo T., Heinz S., 2005, Nature, 436, 819
Gandhi P., Rao A., Johnson M. A. C., Paice J. A., Maccarone T. J., 2019, MNRAS, 485, 2642
Gandhi P. et al., 2011, ApJ, 740, L13
Gandhi P. et al., 2017, Nat. Astron., 1, 859
Gies D., ten Brummelaar T., Schaefer G., Baron F., White R., 2019, BAAS, p. 226
González Hernández J. I., Casares J., 2010, A&A, 516, A58
Gravity Collaboration et al., 2017a, A&A, 602, A94
Gravity Collaboration et al., 2017b, A&A, 602, L11
Gravity Collaboration et al., 2018a, Nature, 563, 657
Gravity Collaboration et al., 2018b, A&A, 615, L15
Gravity Collaboration et al., 2018c, A&A, 618, L10
Gravity Collaboration et al., 2019a, A&A, 623, L11
Gravity Collaboration et al., 2019b, A&A, 625, L10
Gravity Collaboration et al., 2020, A&A, 636, L5,
Greene J., Bailyn C. D., Orosz J. A., 2001, ApJ, 554, 1290
Hammerstein E. K., Cackett E. M., Reynolds M. T., Miller J. M., 2018, MNRAS, 478, 4317
Hillwig T. C., Gies D. R., 2008, ApJ, 676, L37
Hjellming R. M., Rupen M. P., 1995, Nature, 375, 464
Hjellming R. M. et al., 2000, ApJ, 544, 977
Homan J., Buxton M., Markoff S., Bailyn C. D., Nespoli E., Belloni T., 2005, ApJ, 624, 295
Hynes R. I., 2005, ApJ, 623, 1026
Jonker P. G., Nelemans G., 2004, MNRAS, 354, 355
Jonker P. G., Nelemans G., Bassa C. G., 2007, MNRAS, 374, 999
Kalamkar M., Casella P., Uttley P., O'Brien K., Russell D., Maccarone T., van der Klis M., Vincentelli F., 2016, MNRAS, 460, 3284
Kaper L., Lamers H. J. G. L. M., Ruymaekers E., van den Heuvel E. P. J., Zuiderwijk E. J., 1995, A&A, 300, 446
Kawamuro T. et al., 2018, Astron. Telegram, 11399, 1
Khargharia J., Froning C. S., Robinson E. L., 2010, ApJ, 716, 1105
Kishimoto M., Hönig S. F., Antonucci R., Barvainis R., Kotani T., Tristram K. R. W., Weigelt G., Levin K., 2011, A&A, 527, A121
Koljonen K. I. I. et al., 2015, ApJ, 814, 139
Lachaume R., 2003, A&A, 400, 795
Lacour S. et al., 2019, A&A, 624, A99
Lapeyrere V. et al., 2014, in Proc. SPIE Conf. Ser. Vol. 9146, p. 91462D
Laurent P., Rodriguez J., Wilms J., Cadolle Bel M., Pottschmidt K., Grinberg V., 2011, Science, 332, 438
Liska M., Hesp C., Tchekhovskoy A., Ingram A., van der Klis M., Markoff S., 2018, MNRAS, 474, L81
Lopez B. et al., 2014, The Messenger, 157, 5
Lopez L. A., Marshall H. L., Canizares C. R., Schulz N. S., Kane J. F., 2006, ApJ, 650, 338
Maccarone T. J., 2002, MNRAS, 336, 1371
MacDonald R. K. D. et al., 2014, ApJ, 784, 2
Maitra D., Scarpaci J. F., Grinberg V., Reynolds M. T., Markoff S., Maccarone T. J., Hynes R. I., 2017, ApJ, 851, 148
Malzac J. et al., 2018, MNRAS, 480, 2054
Mandal A. K., Singh A., Stalin C. S., Chandra S., Gandhi P., 2018, Astron. Telegram, 11462, 1
Markoff S., 2008, In proc. "Microquasars and Beyond", Available at: http://pos.sissa.it/cgi-bin/reader/conf.cgi?confid=62, preprint (arXiv:0811.3601)
Markoff S., Falcke H., Fender R., 2001, A&A, 372, L25
Markoff S., Nowak M. A., Wilms J., 2005, ApJ, 635, 1203
Masetti N., Bianchini A., Bonibaker J., della Valle M., Vio R., 1996, A&A, 314, 123
McClintock J. E., Remillard R. A., 2006, in Lewin W., van der Klis M., eds, Black Hole Binaries. Compact Stellar X-ray Sources, Cambridge Astrophysics Ser. 39. Cambridge Univ. Press, Cambridge, UK, p. 157
McHardy I. M., Koerding E., Knigge C., Uttley P., Fender R. P., 2006, Nature, 444, 730
Merloni A., Heinz S., di Matteo T., 2003, MNRAS, 345, 1057
Merloni A. et al., 2012, eROSITA Science Book: Mapping the Structure of the Energetic Universe, preprint (arXiv:1209.3114)
Migliari S., Tomsick J. A., Maccarone T. J., Gallo E., Fender R. P., Nelemans G., Russell D. M., 2006, ApJ, 643, L41
Migliari S. et al., 2007, ApJ, 670, 610
Miller-Jones J. C. A., 2014, PASA, 31, e016
Miller-Jones J. C. A., Fender R. P., Nakar E., 2006, MNRAS, 367, 1432
Miller-Jones J. C. A., Jonker P. G., Ratti E. M., Torres M. A. P., Brocksopp C., Yang J., Morrell N. I., 2011, MNRAS, 415, 306
Miller-Jones J. C. A. et al., 2012, MNRAS, 421, 468
Miller-Jones J. C. A. et al., 2019, Nature, 569, 374
Minniti D. et al., 2010, New Astron., 15, 433
Mioduszewski A. J., Rupen M. P., Hjellming R. M., Pooley G. G., Waltman E. B., 2001, ApJ, 553, 766
Mirabel I. F., Dhawan V., Chaty S., Rodriguez L. F., Marti J., Robinson C. R., Swank J., Geballe T., 1998, A&A, 330, L9
Mirabel I. F., Dhawan V., Mignani R. P., Rodrigues I., Guglielmetti F., 2001, Nature, 413, 139
Mirabel I. F., Rodríguez L. F., 1994, Nature, 371, 46
Miroshnichenko A. S., Klochkova V. G., Bjorkman K. S., Panchuk V. E., 2002, A&A, 390, 627
Monnier J. D. et al., 2007, Science, 317, 342
Morris B. M., Agol E., Davenport J. R. A., Hawley S. L., 2018, MNRAS, 476, 5408
Motta S. E. et al., 2017, MNRAS, 471, 1797
Muñoz-Darias T., Motta S., Belloni T. M., 2011, MNRAS, 410, 679
Orosz J. A., McClintock J. E., Aufdenberg J. P., Remillard R. A., Reid M. J., Narayan R., Gou L., 2011b, ApJ, 742, 84
Orosz J. A., Steiner J. F., McClintock J. E., Torres M. A. P., Remillard R. A., Bailyn C. D., Miller J. M., 2011a, ApJ, 730, 75
Orosz J. A. et al., 2001, ApJ, 555, 489
O'Brien K., Horne K., Hynes R. I., Chen W., Haswell C. A., Still M. D., 2002, MNRAS, 334, 426
Paice J. A. et al., 2019, MNRAS, 490, L62
Perlman E. S. et al., 2011, ApJ, 743, 119
Plotkin R. M., Markoff S., Kelly B. C., Körding E., Anderson S. F., 2012, MNRAS, 419, 267
Rahoui F., Lee J. C., Heinz S., Hines D. C., Pottschmidt K., Wilms J., Grinberg V., 2011, ApJ, 736, 63
Rees M. J., 1978, Nature, 275, 516
Rodriguez J. et al., 2015, ApJ, 807, 17
Romero G. E., Boettcher M., Markoff S., Tavecchio F., 2017, Space Sci. Rev., 207, 5
Rushton A. P. et al., 2017, MNRAS, 468, 2788
Russell D. M., Casella P., Kalemci E., Vahdat Motlagh A., Saikia P., Pirbhoy S. F., Maitra D., 2020, MNRAS, preprint (arXiv:2002.08399)
Russell D. M., Fender R. P., Hynes R. I., Brocksopp C., Homan J., Jonker P. G., Buxton M. M., 2006, MNRAS, 371, 1334
Russell D. M., Maitra D., Dunn R. J. H., Markoff S., 2010, MNRAS, 405, 1759
Russell D. M., Shahbaz T., 2014, MNRAS, 438, 2083
Russell D. M. et al., 2013, MNRAS, 429, 815
Russell D. M. et al., 2018, Astron. Telegram, 11533, 1
Russell T. D., Soria R., Miller-Jones J. C. A., Curran P. A., Markoff S., Russell D. M., Sivakoff G. R., 2014, MNRAS, 439, 1390
Russell T. D. et al., 2015, MNRAS, 450, 1745
Russell T. D. et al., 2020, MNRAS, submitted
Saikia P., Russell D. M., Bramich D. M., Miller-Jones J. C. A., Baglio M. C., Degenaar N., 2019, ApJ, 887, 21
Sams B. J., Eckart A., Sunyaev R., 1996, Nature, 382, 47
Shahbaz T., Watson C. A., Dhillon V. S., 2014, MNRAS, 440, 504
Stevens A. L. et al., 2018, ApJ, 865, L15
Stirling A. M., Spencer R. E., de la Force C. J., Garrett M. A., Fender R. P., Ogley R. N., 2001, MNRAS, 327, 1273
Swain M. et al., 2003, ApJ, 596, L163
ten Brummelaar T. A. et al., 2005, ApJ, 628, 453

Tetarenko A. J. et al., 2017, MNRAS, 469, 3141
Thureau N. D. et al., 2009, MNRAS, 398, 1309
Tingay S. J. et al., 1995, Nature, 374, 141
Tomsick J. A., Muterspaugh M. W., 2010, ApJ, 719, 958
Torres M. A. P., Casares J., Jiménez-Ibarra F., Muñoz-Darias T., Armas-Padilla M., Jonker P. G., Heida M., 2019, ApJ, 882, L21
Tucker M. A. et al., 2018, ApJ, 867, L9
Török G., Bakala P., Šrámková E., Stuchlík Z., Urbanec M., 2010, ApJ, 714, 748
van Belle G., Armstrong J. T., Baines E., Llama J., Schmitt H., 2019, BAAS, p. 104
van Oers P. et al., 2010, MNRAS, 409, 763
Vincentelli F. M. et al., 2018, MNRAS, 477, 4524
Waisberg I., Dexter J., Olivier-Petrucci P., Dubus G., Perraut K., 2019b, A&A, 624, A127
Waisberg I., Dexter J., Petrucci P.-O., Dubus G., Perraut K., 2019a, A&A, 623, A47
Waisberg I. et al., 2017, ApJ, 844, 72
Walker R. C., Hardee P. E., Davies F. B., Ly C., Junor W., 2018, ApJ, 855, 128
Weigelt G. et al., 2012, A&A, 541, L9
Zanin R., Fernández-Barral A., de Oña Wilhelmi E., Aharonian F., Blanch O., Bosch-Ramon V., Galindo D., 2016, A&A, 596, A55
Zdziarski A. A., Pjanka P., Sikora M., Stawarz Ł., 2014, MNRAS, 442, 3243

This paper has been typeset from a TEX/LATEX file prepared by the author.